INSTITUTE OF PHYSICS PUBLISHING JOURNAL OF PHYSICS B: ATOMIC, MOLECULAR AND OPTICAL PHYSICS

J. Phys. B: At. Mol. Opt. Phys. **34** (2001) 3287–3300 PII: S0953-4075(01)24179-0

Inner-shell processes of Li- and Be-like Fe

C P Ballance[1], **N R Badnell**[1] **and K A Berrington**[2]

[1] Department of Physics and Applied Physics, University of Strathclyde, Glasgow G4 0NG, UK
[2] School of Science and Mathematics, Sheffield Hallam University, Sheffield S1 1WB, UK

Received 17 April 2001
Published 6 August 2001
Online at stacks.iop.org/JPhysB/34/3287

Abstract

The core-excitation of inner-shell electrons incorporating the effects of radiation damping are investigated within a Breit–Pauli R-matrix framework. Highly ionized Fe species are known to undergo severe damping, both within the context of electron-impact excitation and photoionization. Hence, an $n = 3$ model of Li-like Fe is used to incorporate these effects on the resonance structure associated with the core-excited states produced by the electron-impact excitation of Li-like Fe and the photoionization of Be-like Fe. This work forms part of the RmaX Network, whose objectives include the study of inner-shell electron-impact excitation and photoionization processes, and is highly relevant to studies utilizing observations from the high-resolution x-ray satellites *Chandra* and *XMM–Newton*.

(Some figures in this article are in colour only in the electronic version; see `www.iop.org`)

1. Introduction

The core-excitation of atomic systems by an incident electron of several hundred Rydbergs can be categorized as a soft x-ray transition. We are interested in examining the electron-impact excitation and photoionization of highly ionized systems in this energy regime and, in particular, modelling accurately the resonance structure that arises in these cross sections. It is intended that this theoretical groundwork will be utilized to support the analysis of spectral observations made by the recently launched x-ray satellites *Chandra* and *XMM–Newton*. The emission line project associated with *Chandra* would like effective collision strengths and partial photoionization cross sections for astrophysically abundant elements, especially Fe. We have already modelled outer-shell transitions in Li- and Be-like Fe in large-scale R-matrix calculations (Berrington *et al* 1995). These should provide excitation rate coefficients within their 'primary temperature range of 10^5–10^8 K' and so the focus of this paper is on inner-shell transitions. To this end, we note that recent advances in the implementation of the R-matrix outer-region theory (Robicheaux *et al* 1995) now allow for radiationally damped photoionization cross sections from bound states other than the ground state.

Previously, Tully *et al* (1990) and Berrington *et al* (1997) have investigated photoionization of the beryllium sequence, including iron. Tully *et al* (1990) implemented a five-term LS-coupling $n = 3$ model for Li-like ions and generated oscillator strengths and low-energy photoionization cross sections from the respective $1s^2 2s^2$ Be-like ground states. The corresponding Iron Project paper for electron-impact excitation involved an $n = 4$ Breit–Pauli calculation (Berrington and Tully 1997). Their 15-level calculation highlighted the role of resonances in relation to the earlier distorted wave results of Zhang *et al* (1990b). The study of Berrington and Tully was strictly for outer-shell transitions. This enabled them to span an electron-impact energy of 265 Ryd and to present thermally averaged (effective) collision strengths up to 10^8 K. Berrington *et al* (1995) improved upon the photoionization calculation by including core-excited states (albeit using only the 1s–2p orbitals), as well as pseudo-states so as to account for double-ionization possibilities.

Black *et al* (1997) also included core-excited states in their photoionization study, but omitted those states resulting from the $1s2l3l'$ configurations. Furthermore, as their work was carried out within LS-coupling, they were able to omit the quartet states from their Li-like target representation. We have to include these states so as to ensure completeness within our intermediate coupling calculation. Our extended calculation will provide new resonance-resolved collision strengths to the 1s2s3l and 1s2p3l configurations and will reveal resonance structure in the 480–560 Ryd regime.

In this regime, we can make comparisons with the early work of Sampson and colleagues who tabulated fits to core-excited collision strengths for the transitions $1s^2 2l - 1s2l2l'$ (Sampson *et al* 1979, 1985a) and $1s^2 3l - 1s2l3l'$ (Sampson *et al* 1985b). They employed the Coulomb–Born exchange method. This should give background cross sections comparable to those from our own work. As results for outer-shell excitations of Li-like Fe have been presented before, our primary focus shall be on the inner-shell transitions. Excitation of these hollow states can populate quartet LS-terms. These can only decay through spin–orbit interactions and so have relatively long lifetimes. Also, the first $1s2l2l'$ core-excited states, especially the quartet terms, will support Rydberg series of resonances that are only weakly autoionizing and so will be subject to strong radiation damping.

Apart from the present study, a common deficiency of all of the aforementioned work is the omission of the effect of radiation damping. This can greatly reduce the resonant enhancement of cross sections which, in weak transitions, inevitably reduces the effective collision strength or integrated photoionization cross section. This work also forms part of the RmaX Network[3], whose objectives include the study of inner-shell electron-impact excitation and photoionization processes.

The structure of this paper is as follows. In section 2 we review briefly the theory behind the optical potential approach to allow for radiation damping within the R-matrix method. In section 3 we give details of our calculational approach for both inner-shell electron-impact excitation and photoionization. In section 4 we present illustrative results and compare the background cross sections with those of Cunto *et al* (1993) for photoionization and with Sampson *et al* (1979) for electron-impact excitation. We finish with a short conclusion.

2. Theory

The foundation of both the radiation-damped excitation and photoionization calculations is the standard R-matrix package of Berrington *et al* (1995). However, unlike typical electron-impact excitation calculations, $(N + 1)$-electron dipole matrix elements between symmetries

[3] http://amdpp.phys.strath.ac.uk/UK_RmaX

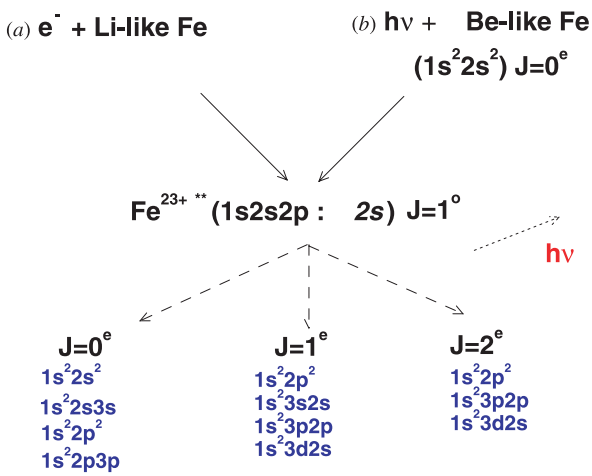

Figure 1. Illustration of the dominant radiative damping pathways for the 1s2s2p : ns resonance (for $n = 2$, $J^\pi = 1^\mathrm{o}$).

of low total angular momentum J will be required. These dipole matrix elements are the cornerstone of the optical potential approach (Robicheaux *et al* 1995) which enables resonances to decay through photon emission to a bound state. In the case of Be-like photoionization, the prerequisite $J^\pi = 0^\mathrm{e}$–1^o dipole also needs to be supplemented by $J^\pi = 1^\mathrm{o}$–2^e and $J^\pi = 1^\mathrm{o}$–1^e dipoles to allow access to radiatively accessible bound states resulting from these symmetries (see figure 1 for an illustration). The resonance lifetime is inversely proportional to its width and consequently, without radiation damping, the higher members of any Rydberg series have increasingly unphysical lifetimes. Heavy, highly ionized species in particular are subject to acute radiation damping from the first member of a Rydberg series, as illustrated in figure 2.

It is convenient to make a distinction between the damping of resonances to final states which are fully contained within our R-matrix hypersphere, and those which lie predominantly outside. The former have the optical potential implemented through a complex R-matrix of the form, and are categorized as type IIS (Robicheaux *et al* 1995),

$$R_{ij} = \tfrac{1}{2}\sum_k \frac{w_{ik}w_{jk}}{E_k - E} - \sum_{kk'nn'} w_{ik}w_{jk'}\gamma^{-1}\frac{\langle k||\nabla||n\rangle\langle k'||\nabla||n'\rangle}{(E_k - E)(E_{k'} - E)} \tag{1}$$

in which the second summation introduces the complex damping term. The $\boldsymbol{w}_{jk'}$ and $\boldsymbol{E}_{k'}$ are the surface amplitudes and R-matrix poles of those symmetries associated with bound-state formation. The γ^{-1} is a small inverted complex matrix that is given explicitly by equation (100) of Robicheaux *et al* (1995). An example in Li-like Fe is the damping of the 'correlation resonances' that arise in the photorecombination process described by

$$\mathrm{e}^- + 1\mathrm{s}^2 2\mathrm{s} \rightarrow 1\mathrm{s}2\mathrm{s}2\mathrm{p}^2 \rightarrow 1\mathrm{s}^2 2\mathrm{s}2\mathrm{p} + \gamma$$

where the final state must be bound relative to the ground state. The inverse (right-to-left) process is photoionization.

When the final state is not fully contained within the R-matrix hypersphere, then damping can be readily implemented through MQDT (multi-channel quantum defect theory) as implemented by Gorczyca and Badnell (2000). (This is not the case for correlation resonances since they arise in the open–open part of the unphysical collision matrix.) Inner-electron damping (type I), e.g.

$$\mathrm{e}^- + 1\mathrm{s}^2 2\mathrm{s} \rightarrow 1\mathrm{s}2\mathrm{s}2\mathrm{p}nl \rightarrow 1\mathrm{s}^2 2\mathrm{s}nl + \gamma$$

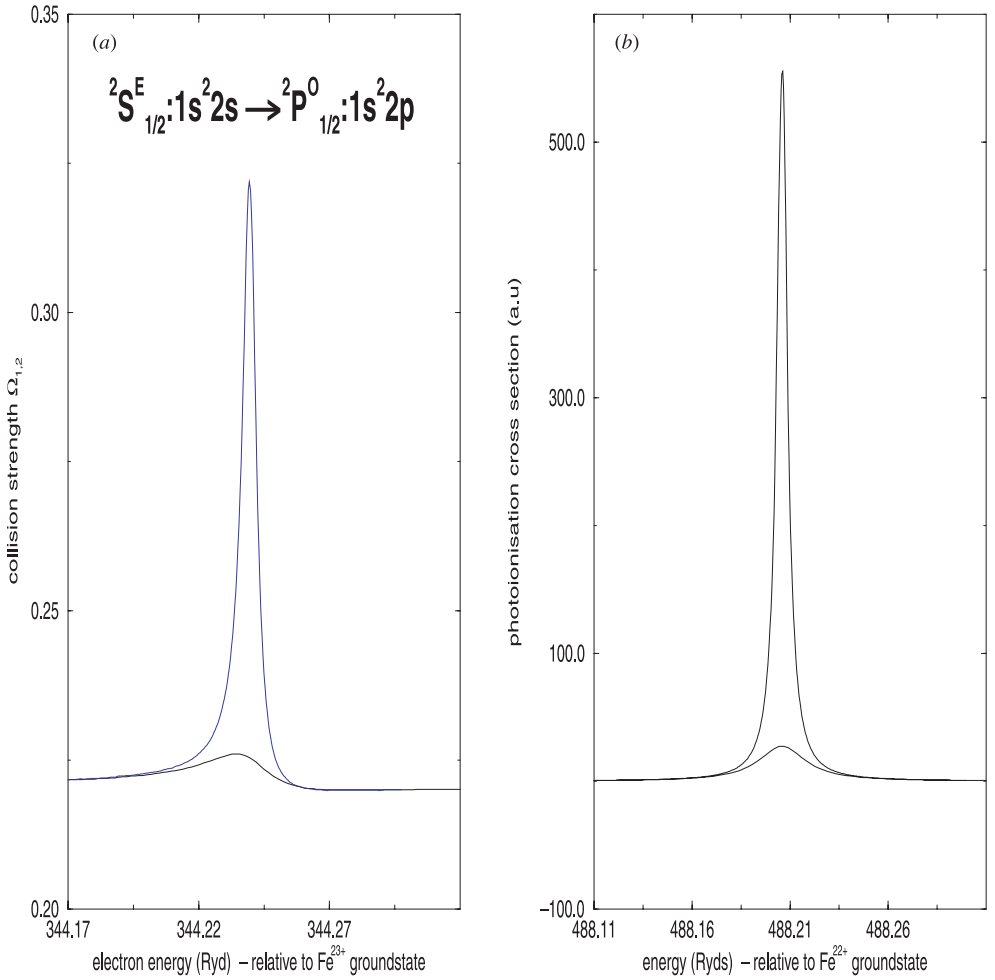

Figure 2. Damped and undamped electron-impact excitation collision strengths (*a*) and photoionization cross sections (*b*) focusing on the 1s2s2p : *n*s resonance (for $n = 2$, $J^\pi = 1^o$).

i.e. the Rydberg electron is considered to be unperturbed, is taken into account through the use of a complex effective quantum number, namely $\nu_c = \nu/(1 - i\Gamma_r\nu^2/z^2)^{1/2}$, where Γ_r is the core radiative width. Finally, Rydberg–Rydberg damping (type IIL) is incorporated as a perturbation on the unphysical K-matrix using equation (116) of Robicheaux *et al* (1995). An example is given by

$$e^- + 1s^2 2s \rightarrow 1s^2 2pnl \rightarrow 1s^2 2pn'l' + \gamma.$$

3. Calculation

We used AUTOSTRUCTURE (Badnell 1986) to generate the 1s–3d bound atomic orbitals to be employed in our description of the target. Configurations of the form $1s^2nl$ and $1snln'l'$ with $n, n' \leqslant 3$, but omitting $1s3l3l'$, result in the formation of 90 intermediate coupling levels. Comparisons with the NIST database (NIST http://physics.nist.gov) show energy levels and

Table 1. Some energy levels (Ryd) in Li-like Fe^{23+}.

Level	Configuration	J	Present	NIST[a]	Difference[b] (%)
1	$1s^2 2s$	$\frac{1}{2}$	0.00	0.00	0.00
2	$1s^2 2p$	$\frac{1}{2}$	3.62	3.57	1.38
3	$1s^2 2p$	$\frac{3}{2}$	4.74	4.75	0.21
4	$1s^2 3s$	$\frac{1}{2}$	84.49	84.50	0.01
5	$1s^2 3p$	$\frac{1}{2}$	85.46	85.45	0.01
6	$1s^2 3p$	$\frac{3}{2}$	85.80	85.81	0.01
7	$1s^2 3d$	$\frac{3}{2}$	86.19	86.19	0.00
8	$1s^2 3d$	$\frac{5}{2}$	86.30	86.31	0.001
9	$1s2s^2$	$\frac{1}{2}$	486.08	—	—
10	1s2s2p	$\frac{1}{2}$	487.05[c]	488.95	0.39
11	1s2s2p	$\frac{3}{2}$	487.35[c]	489.82	0.5

[a] NIST database (http://physics.nist.gov).
[b] Relative to the present results.
[c] Zhang *et al* (1990a) give eigenenergies for $[^4P_{1/2,3/2}]$ of 487.0, 487.1 Ryd.

autoionization rates in good accord with our own—see table 1. The low-lying level energies all agree to within about 1%, whilst the higher-lying levels differ by at most 0.5%.

Our R-matrix inner-region calculation used 18 continuum basis orbitals per angular momentum and this ensures that the scattering model is complete up to an incident electron energy of 769 Ryd. Our initial 43 LS-coupling N-electron terms underwent spin–orbit splitting to reproduce the same 90 intermediate coupling level energies given by AUTOSTRUCTURE. The maximum L for the $(N+1)$-electron LS-coupling Hamiltonians was set at 6. This enables Breit–Pauli R-matrix results to be computed up to $J = 4$. The LS-coupling Hamiltonian matrix size was purposely restricted to a dimension of $\approx$1500 because even these LS-coupling symmetries give rise to J-resolved matrices of order ≈ 7000. We partitioned the inner-region calculation into a run of low maximum J so as to produce dipole matrix elements and another to higher maximum J for converged excitation cross sections so as to minimize the CPU time and disc space required. This ensures that the dominant resonance structure undergoes damping, whilst no time is wasted on higher non-resonant partial waves. $J = 4$ does not provide enough partial waves to converge low-lying dipole transitions so, rather than repeatedly diagonalize large Breit–Pauli Hamiltonians, we used the intermediate coupling frame transformation (ICFT) approach of Griffin *et al* (1998). This entails transforming unphysical S- or K-matrices (within the framework of MQDT) to a jK-coupling scheme before a further transformation, involving term-coupling coefficients (TCCs), gives rise to intermediate coupling level-to-level excitation cross sections. It is also assumed that the original LS-coupling inner-region calculation included the mass–velocity and Darwin operators, and that the N-electron terms undergo spin–orbit mixing to provide the TCCs. LS-coupling partial waves ($L = 3$–30) then supplemented the calculation to $J = 4$ with the contributions from $J = 5$–28.

The code STGB (Seaton, unpublished) was used to identify those J-resolved bound states of Be-like Fe which lie strictly below the Li-like ground state. Table 2 gives the configuration,

Table 2. J^{π} bound levels of Be-like Fe^{22+}.

Configuration	Symmetry	Threshold	n	Photoionization[a]
$1s^2 2s : ns$	0^e	1	1.917	⋆
$1s^2 3s : ns$	0^e	4	1.900	⋆
$1s^2 2p : np$	0^e	2	1.952	⋆
$1s^2 2p : np$	0^e	3	1.975	⋆
$1s^2 3p : np$	0^e	5	1.930	⋆
$1s^2 3p : np$	0^e	6	1.943	⋆
$1s^2 3p : ns$	0^o	5	1.901	—
$1s^2 2s : np$	0^o	1	1.941	—
$1s^2 3s : np$	0^o	4	1.925	—
$1s^2 3d : np$	0^o	7	1.940	—
$1s^2 3s : ns$	1^e	4	1.898	⋆
$1s^2 3d : ns$	1^e	7	1.904	⋆
$1s^2 2p : np$	1^e	3	1.952	⋆
$1s^2 3p : np$	1^e	5	1.925	⋆
$1s^2 3p : np$	1^e	5	1.929	⋆
$1s^2 3p : np$	1^e	6	1.932	⋆
$1s^2 3p : np$	1^e	6	1.934	⋆
$1s^2 2p : ns$	1^o	2	1.919	—
$1s^2 3p : ns$	1^o	5	1.903	—
$1s^2 2s : np$	1^o	1	1.967	—
$1s^2 3s : np$	1^o	4	1.926	—
$1s^2 3s : np$	1^o	4	1.935	—
$1s^2 3p : np$	1^o	7	1.932	—
$1s^2 3p : np$	1^o	7	1.939	—
$1s^2 3p : np$	1^o	7	1.944	—
$1s^2 2s : np$	1^o	1	2.950	—
$1s^2 3d : ns$	2^e	7	1.904	⋆
$1s^2 3d : ns$	2^e	8	1.908	⋆
$1s^2 2p : np$	2^e	3	1.955	⋆
$1s^2 2p : np$	2^e	3	1.963	⋆
$1s^2 3p : np$	2^e	5	1.929	⋆
$1s^2 3p : np$	2^e	6	1.934	⋆
$1s^2 3p : np$	2^e	6	1.938	⋆
$1s^2 2p : ns$	2^o	3	1.917	—
$1s^2 3p : ns$	2^o	6	1.901	—
$1s^2 3p : ns$	2^o	6	1.934	—
$1s^2 3d : np$	2^o	7	1.928	—
$1s^2 3d : np$	2^o	8	1.936	—
$1s^2 3d : np$	2^o	8	1.939	—
$1s^2 2p : ns$	2^o	3	2.923	—
$1s^2 3d : ns$	3^e	8	1.904	—
$1s^2 3p : np$	3^e	6	1.933	—
$1s^2 3d : np$	3^o	7	1.931	—
$1s^2 3d : np$	3^o	8	1.937	—
$1s^2 3d : np$	3^o	8	1.942	—
$1s^2 3d : np$	4^o	8	1.935	—

[a] The ⋆ denotes bound states that are radiatively accessible in photoionization.

J-symmetry and effective quantum number of the states identified. All of these states contribute to damped electron-impact excitation, but the final column indicates whether or not they also contribute to damped photoionization. Previous photoionization calculations (Gorczyca 2000) from closed-shell ground states only required a single dipole symmetry, namely $0^e \rightarrow 1^o$, but now we must allow for damping transitions resulting from $J^\pi = 1^e, 2^e$ bound-state symmetries, as well as for higher members of the 0^e. Only the ground and first excited states can support bound $n = 3$ members, which reduces their numbers considerably.

Subsequently, the recently developed codes STGFDAMP (Gorczyca and Badnell 1996) and STGBF0DAMP[4] (Badnell, unpublished) were used to calculate electron-impact excitation and photoionization cross sections to the core-excited $1snln'l'n''l''$ states, as well as gauging the effects of radiation damping on the resonance structure.

4. Results

Figure 3 first demonstrates that our total background photoionization cross section compares favourably with the TOPbase values (Cunto *et al* 1993), at least over a coarse broad-sweep of photon energy.

We next look into the detailed resonance structure. A fully resolved single 1s2s2p : 2s ($J^\pi = 1^o$) resonance was selected to illustrate the consistent amount of damping, both within excitation and photoionization. This is the first member of a Rydberg series and can be categorized as a 'correlation resonance'. As a result, its damping comes predominantly from the complex R-matrix. Figure 1 shows the bound states that are radiatively accessible by dipole selection rules, regardless of whether the resonance was formed by excitation or photoionization. The collision strength and photoionization cross section (figure 2) are damped by almost a factor of 30.

We now look at the extent of damping involved with two sets of $n = 3$ resonances. We are purposely looking at one set of resonances below, and another above, the first group of $1s2l2l'$ levels. Those resonances that lie below are in a similar situation to the photoionization/excitation comparison whereby they experience extreme damping due to there being no easily accessible autoionization channels. However, those above the first group of hollow excited states can autoionize into the $1s2l2l'$ continuum, hence maintaining a prominent structure. Figure 4 illustrates how the resonances attached to $1s2l3l'$ states have access to more autoionization pathways, as opposed to those attached to the $1s2l2l'$ states. Figure 5 illustrates the resultant effect on the resonances formed during photoionization.

Comprehensive electron-impact excitation collision strengths from the ground state to all levels of the $1s2l2l'$ configurations are presented in figures 6–8. The broken curves within these graphs denote the results from a simpler $n = 2$ model, i.e. one that omits the $n = 3$ configurations. Although lacking resonance structure above 495 Ryd, it does provide convergence checks on the more elaborate $n = 3$ model because the contribution from higher J-symmetries is more easily computed. As the energy-level separations are large, the cross sections converged quickly and gave consistent results between the two models. Not surprisingly, the strongest transition for this grouping of $1s2l2l'$ states is the $1s^2 2s\ ^2S_{1/2}$–$1s2s2p\ ^2P^o_{3/2}$, although the $^4P^o_J$ are significant also. Independent comparisons from the ground state were carried out with the collected works of Sampson and colleagues.

[4] The code STGBF0DAMP is not a damped version of the general undamped STGBF code since it still requires that the initial photoionizing state be fully contained within the R-matrix hypersphere, but that is its only restriction.

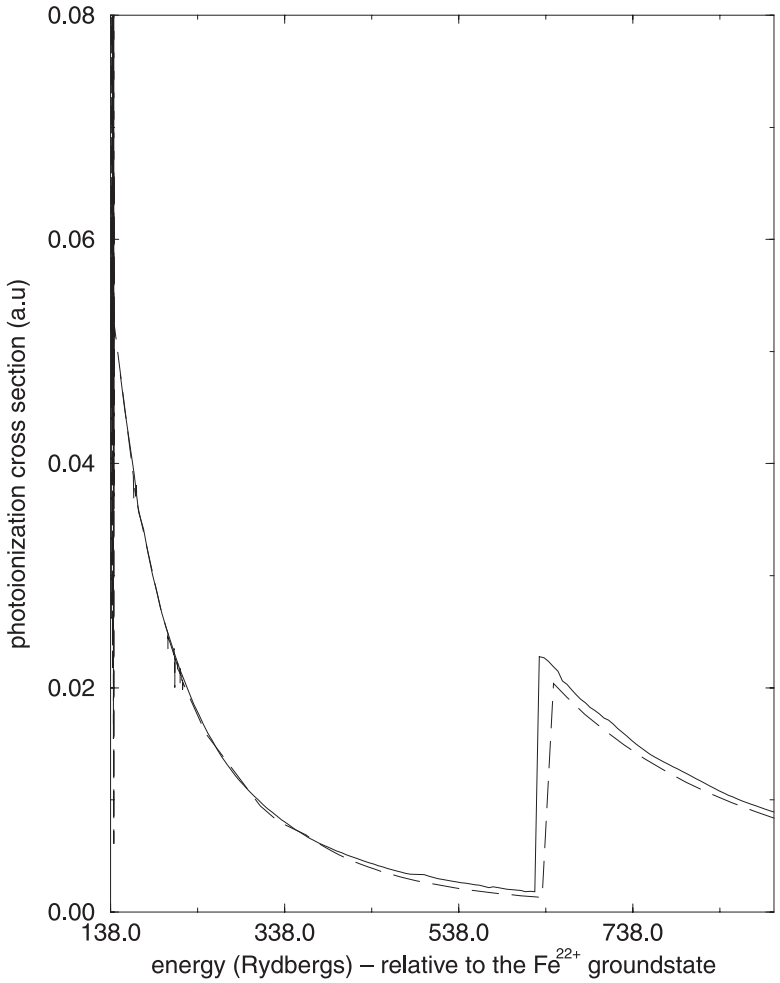

Figure 3. Total photoionization cross section of Be-like Fe for energies from the Li-like ground-state threshold up to 800 Ryd. Full curve, present results; broken curve, TOPbase results (Cunto *et al* 1993). Note that the coarse energy mesh masks the higher-lying resonance structure.

For certain transitions, the intermediate coupling collision strength can be expressed as the multiple of a Z-scaled hydrogenic collision strength (equation (17), Sampson *et al* 1979) namely

$$Z^2\Omega_{\rm IC}(1{\rm s}^2 2{\rm s}\ ^2{\rm S}_{1/2} - A_i) = a(A_i)Z^2\Omega_{\rm H}(1{\rm s}\text{–}2{\rm s}). \tag{2}$$

The A_i refer to the four $1{\rm s}2l2l'$ levels with an overall $J^\pi = \frac{1}{2}^{\rm e}$ symmetry, whilst the scaled hydrogenic collision strengths are tabulated in table III.a of Sampson *et al* (1985a). The coefficients $a(A_i)$ themselves are given in table 2 of Sampson *et al* (1979). Comparisons are also made with these results in figures 6–8. We also make comparisons in figures 6 and 7 for the three $J^\pi = \frac{1}{2}^{\rm e}\text{–}\frac{3}{2}^{\rm o}$ collision strengths, which Sampson *et al* (1979) denote as class E. Their fitting expression is given by

$$Z^2\Omega_{\rm IC}(1{\rm s}^2 2{\rm s}\ ^2{\rm S}_{1/2} - E_i) = a(E_i)Z^2\Omega_{\rm H}(1{\rm s}\text{–}2{\rm p}) + a^{\rm e}(E_i)Z^2\Omega^{\rm e}_{\rm H}(1{\rm s}\text{–}2{\rm p}). \tag{3}$$

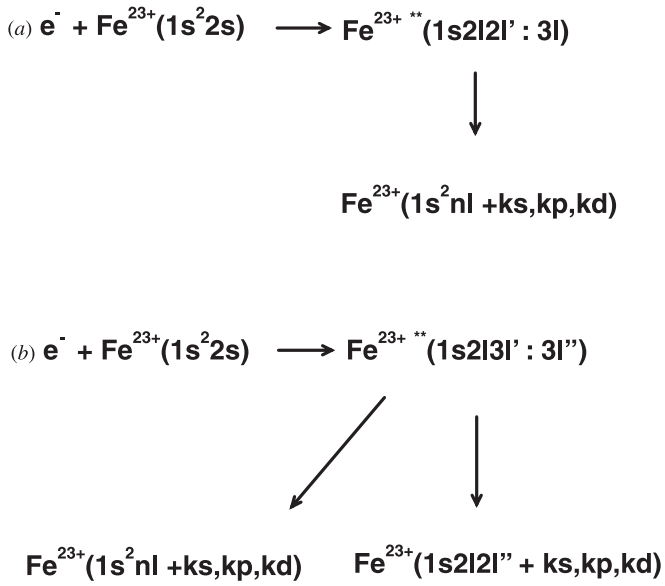

Figure 4. Illustration of the increased autoionization channels available to the $1s2l3l' : 3l''$ (b) as opposed to the $1s2l2l' : 3l''$ resonances (a).

The E_i refer to the three $1s2l2l'$ levels with an overall $J^\pi = \frac{3}{2}^o$ symmetry and the $a(E_i)$ and $a^e(E_i)$ are given in table 3 of Sampson *et al* (1979)[5].

Since the calculations of Sampson *et al* (1979) span quite extensive energy regions, there are only a limited number of points that overlap with the present study. However, these are enough to demonstrate the consistency of the background collision strengths (see figures 6–8). Strictly speaking, x-ray transitions are the primary concern of the RmaX Network but we also want to provide effective collision strengths for outer-shell transitions over $T = 10^4$–10^7 K, for completeness. This necessitated us computing collision strengths up to 600 Ryd. Hence, considerable effort went into converging the $\delta n = 0$ transitions ($1s^2nl \rightarrow 1s^2nl'$). Fortunately, a combination of the exchange LS-coupling R-matrix codes and the ICFT approach enables us to generate results efficiently for symmetries of high angular momentum. In this case, we used the ICFT codes for $J > 4$. Of course, in more complex targets it would be more beneficial to implement a non-exchange calculation at slightly more than twice the highest L-term.

Figures 8(b)–(g) best exemplify cases where a dense forest of narrow resonances are superimposed upon a negligible background collision strength, which is of the order 10^{-5}–10^{-6}. It is in this situation that the resonance structure has its largest effect upon effective collision strengths.

In all of the transitions in figures 6–8, we note the general trend of high $1s2l2l'nl''$ resonances being severely damped in relation to the subsequent $1s2l'3l''nl'''$ groups of resonances. Undamped calculations having 16 hollow $n = 2$ thresholds in a compact energy region could lead to high series members straddling thresholds, which could lead to the effective collision strengths being seriously overestimated. However, now that radiation damping has been implemented, these high members are largely smeared-out for $n > 5$, resulting in more reliable results.

[5] Sampson *et al* (1979) use the superscript 'e' to denote the contribution from electron exchange.

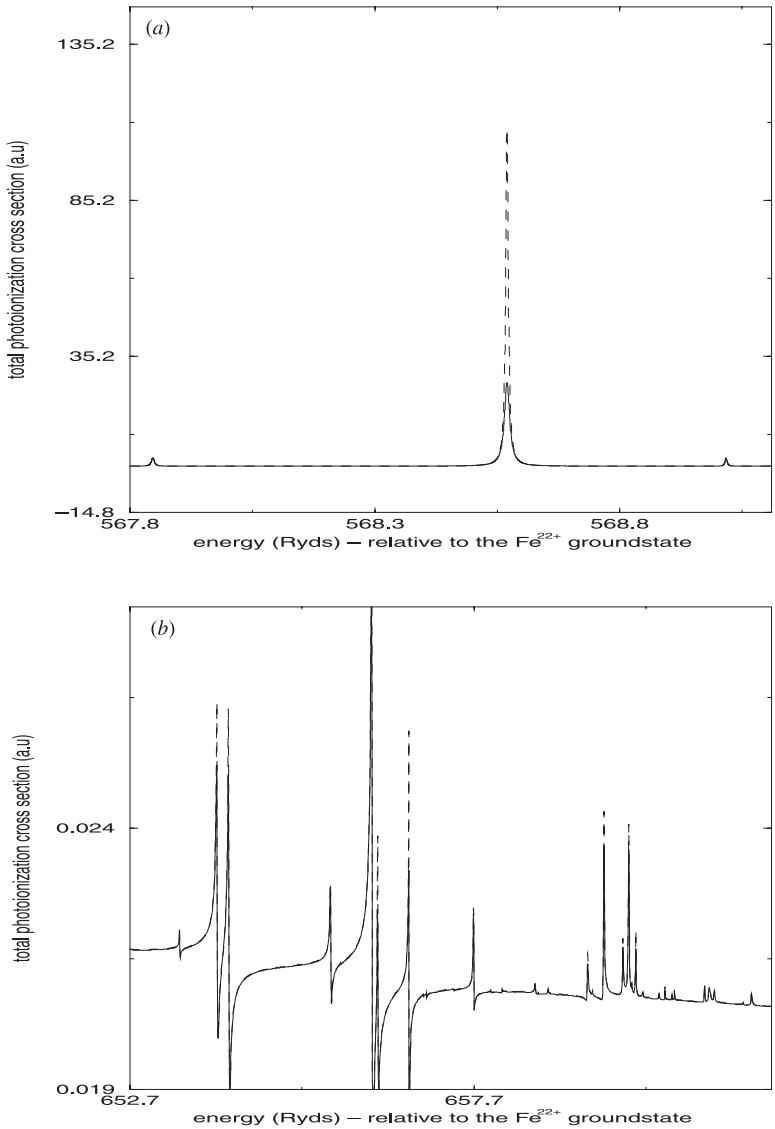

Figure 5. Photoionization cross sections, focusing on $n = 3$ resonances attached to 1s2l2l' (*a*) and 1s2l3l' (*b*) thresholds. The full curves denoted damped results and the broken curves denote undamped results.

According to Shull and Van Steenberg (1982), the coronal abundance of Li-like Fe occurs at approximately $10^{7.25}$ K. Our calculation would need to exceed an electron-impact energy of 1500 Ryd to guarantee converged effective collision strengths here. Therefore, we have appended the 1.9, 2.5 and 4.0 times threshold Z-scaled collision strengths of Sampson *et al* (1985a) to our own. Results for temperatures ranging from 3×10^4 to 3×10^7 K are given in table 3. We note that the values in the 3×10^4 to 3×10^6 K temperature range are derived solely from our own data.

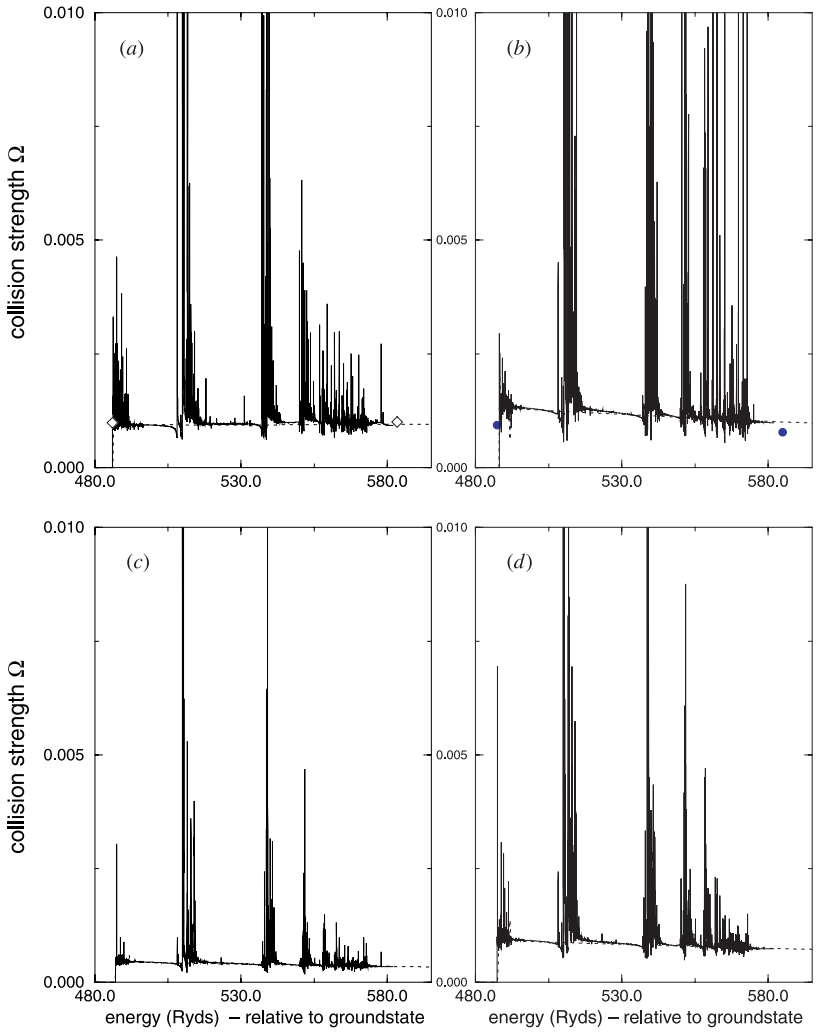

Figure 6. Radiation-damped electron-impact excitation collision strengths from the ground level of Li-like Fe to the $1s2l2l'$ core-excited states. The $1s^2 2s$–$1s2s^2\ ^2S^e_{1/2}$, $1s2s2p\ ^4P^o_{3/2,1/2,5/2}$ transitions are depicted in (*a*)–(*d*), respectively. Full curve, the present $n = 3$ model; dotted curve, the present $n = 2$ model; diamonds, $\delta J = 0$ extracted from Sampson *et al* (1979); circles, $\delta J = 1$ extracted from Sampson *et al* (1979).

Table 3. Effective collision strengths (Υ) from the ground level of Fe^{23+} to selected levels of the $1s2l2l'$ configurations.

$\Upsilon(1-j)$	3×10^4 K[a]	3×10^5 K[a]	3×10^6 K[a]	3×10^7 K[b]
1–9	0.000 22	0.002 17	0.022 20	0.225 108
1–15	0.000 002	0.000 019	0.000 316	0.002 925
1–21	0.000 002	0.000 014	0.000 222	0.001 638
1–24	0.000 012	0.000 118	0.001 414	0.014 301

[a] Present work.
[b] Including high-energy points from Sampson *et al* (1985a).

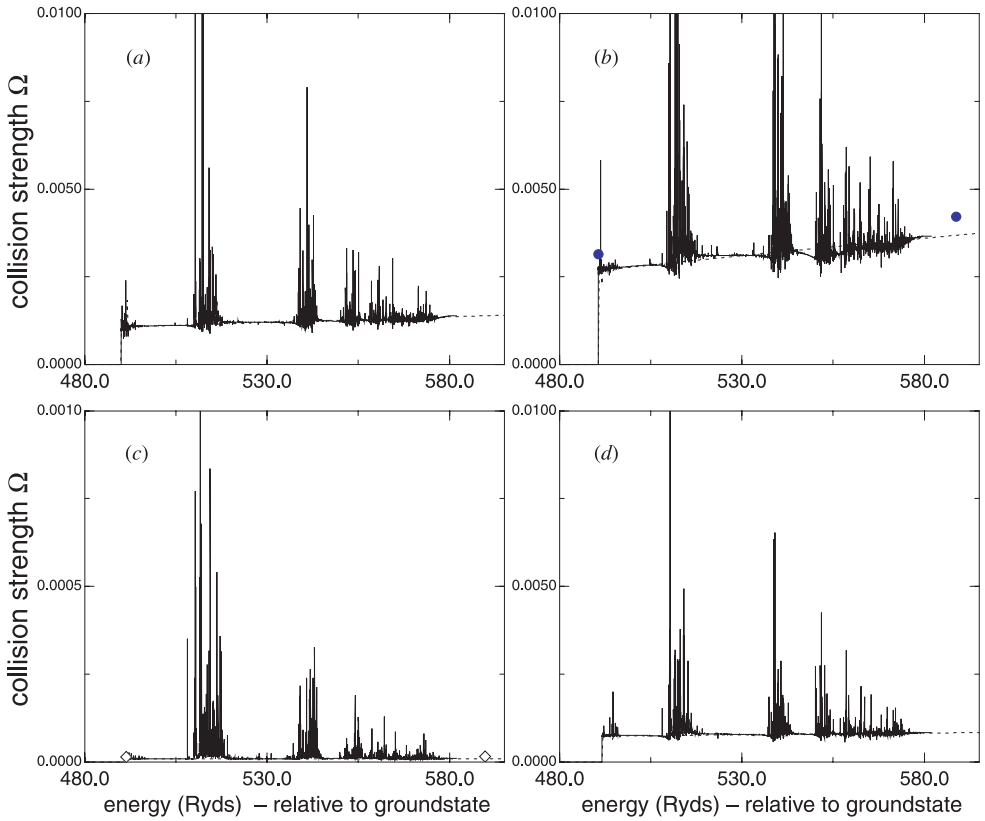

Figure 7. Radiation-damped electron-impact excitation collision strengths from the ground level of Li-like Fe to the $1s2l2l'$ core-excited states. The $1s^2 2s$–$1s2s2p\ ^2P^o_{1/2,3/2}$, $1s2p^2\ ^4P^e_{1/2}$, $1s2s2p\ ^2P^o_{1/2}$ transitions are depicted in (*a*)–(*d*), respectively. Full curve, the present $n = 3$ model; dotted curve, the present $n = 2$ model; diamonds, $\delta J = 0$ extracted from Sampson *et al* (1979); circles, $\delta J = 1$ extracted from Sampson *et al* (1979).

5. Conclusion

A study of the electron-impact excitation of Li-like Fe, and the photoionization of Be-like Fe, has been undertaken which includes the effects of radiation damping. For electron-impact excitation, we have concentrated on transitions from the ground state since 90 levels give rise to collision strengths for 4005 transitions, which would be difficult to present concisely[6]. However, the $1s2l2l'$ configurations provide a range of different types of transitions and enabled us to compare the background cross sections with the results of a simpler $n = 2$ model. Furthermore, as the dipole matrix elements are being produced for damped electron-impact excitation, it seemed prudent to take a single resonance and ensure that it undergoes a similar amount of damping from a photoionization perspective. Our results show that resonances attached to the first grouping of $1s2l2l'$ states undergo the most severe damping and that all resonances are correctly damped near their associated threshold. We believe that this is the first calculation to include resonant structure within transitions to $1s2l2l'$ which, due to the

[6] The full set of results for energy levels, dipole radiative rates and effective collision strengths, tabulated in the atomic data and analysis structure (ADAS) *ADF04* format (Summers 1999), is available via the WWW under http://www-cfadc.phy.ornl.gov/data_and_codes.

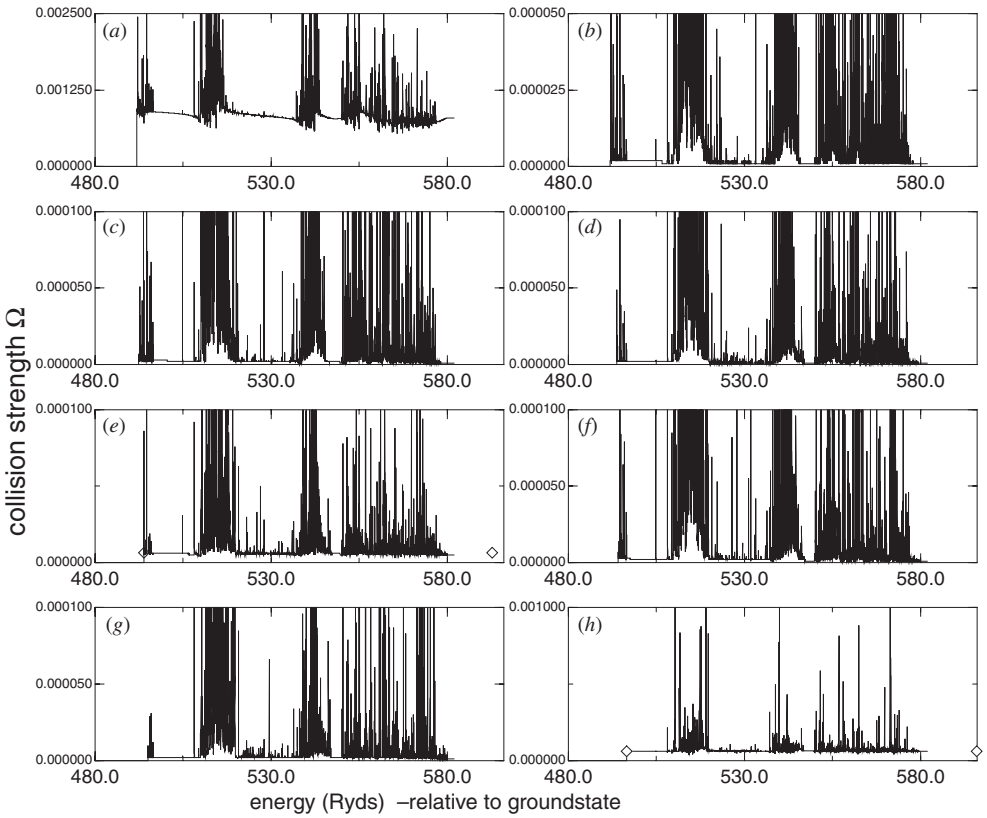

Figure 8. Radiation-damped electron-impact excitation collision strengths from the ground level of Li-like Fe to the $1s2l2l'$ core-excited states. The $1s^2 2s$–$1s2p^2\ {}^4P^e_{3/2}$, $1s2s2p\ {}^2P^o_{3/2}$, $1s2p^2\ {}^4P^e_{5/2}$, ${}^2D^e_{3/2}$, ${}^2P^e_{1/2}$, ${}^2D^e_{5/2}$, ${}^2P^e_{3/2}$, ${}^2S^e_{1/2}$ transitions are depicted in (*a*)–(*h*), respectively. Full curve, the present $n = 3$ model; dotted curve, the present $n = 2$ model; diamonds, $\delta J = 0$ extracted from Sampson *et al* (1979); circles, $\delta J = 1$ extracted from Sampson *et al* (1979).

weak background collision strength of some soft x-ray transitions, can have a significant effect upon the effective collision strength.

Our results for photoionization appear to confirm the assertion of Black *et al* (1997) that, in the case of *total* photoionization from the ground state of highly charged systems, the background cross section is similar whether LS- or intermediate coupling is used. Gorczyca *et al* (2001) have reported similar findings for the L-shell edge in Fe^{14+}.

As part of the remit of the RmaX Network, we are currently focusing on inner-shell photoionization for near neutral Fe systems, as well as the isonuclear neon sequence so as to identify trends due to core excitation. These are more complex models that also have L- and M-shell edges that need to be taken into consideration, rather than only the K-shell edge considered here.

In the future, we would like to include the $1s3l3l'$ states and span an excitation energy range 4 to 5 times greater than used presently. This would fully incorporate the role of resonances associated with these core-excited states in the $15–30 \times 10^6$ K temperature range.

Acknowledgment

The work of the UK RmaX Network is supported by PPARC.

References

Badnell N R 1986 *J. Phys. B: At. Mol. Phys.* **19** 3827–35
Berrington K A, Eissner W and Norrington P N 1995 *Comput. Phys. Commun.* **92** 290–420
Berrington K A, Pelan J C and Quigley L 1997 *J. Phys. B: At. Mol. Opt. Phys.* **30** 4973–90
Berrington K A and Tully J A 1997 *Astron. Astrophys. Suppl.* **126** 105–11
Black G M, Bell K L and Keenan F P 1997 *Astron. Astrophys.* **322** 359–63
Cunto W, Mendoza C, Ochsenbein F and Zeippen C 1993 *Astron. Astrophys.* **275** L5–8
Griffin D C, Badnell N R and Pindzola M S 1998 *J. Phys. B: At. Mol. Opt. Phys.* **31** 3713–27
Gorczyca T W 2000 *Phys. Rev.* A **61** 024702
Gorczyca T W and Badnell N R 1996 *J. Phys. B: At. Mol. Opt. Phys.* **29** L283–90
——2000 *J. Phys. B: At. Mol. Opt. Phys.* **33** 2511–23
Gorczyca T W, Felfli Z, Deb N C and Msezane A Z 2001 *Phys. Rev.* A **63** 010702
Robicheaux F, Gorczyca T W, Pindzola M S and Badnell N R 1995 *Phys. Rev.* A **52** 1319–33
Sampson D H, Clark R E H and Parks A D 1979 *J. Phys. B: At. Mol. Phys.* **12** 3257–72
Sampson D H, Goett S J, Petrou G V, Zhang H and Clark R E H 1985a *At. Data Nucl. Data Tables* **32** 343–402
Sampson D H, Petrou G V, Goett S J and Clarke R E H 1985b *At. Data Nucl. Data Tables* **32** 403–33
Shull J M and Van Steenberg M 1982 *Astron. Astrophys. Suppl.* **48** 85–107
Summers H P 1999 *ADAS User Manual Version 2.1* http://adas.phys.strath.ac.uk
Tully J A, Seaton M J and Berrington K A 1990 *J. Phys. B: At. Mol. Opt. Phys.* **23** 3811–37
Zhang H L, Sampson D H and Clark R E H 1990a *Phys. Rev.* A **41** 198–206
Zhang H L, Sampson D H and Fontes C J 1990b *At. Data Nucl. Data Tables* **44** 31–70